Local Structure Variation, Phase Stability and Electrocatalytic Activity in Rocksalt and Spinel based Multi-Component (CoCuMgNiZn)-Oxide and its Derivatives

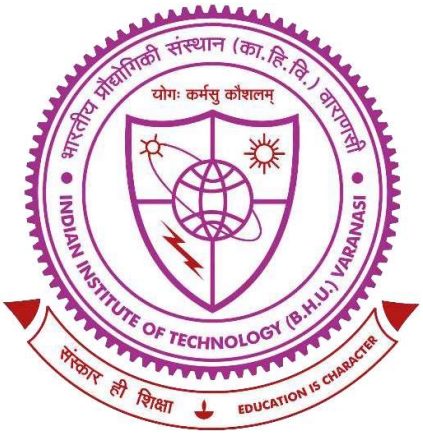

Thesis submitted in partial fulfilment for the

Award of Degree

DOCTOR OF PHILOSOPHY

By

SAPTARSHI MUKHERJEE

Department of Metallurgical Engineering

Indian Institute of Technology

Banaras Hindu University (BHU)

Varanasi – 221005

UP, India

Roll No. 17141502 **2024**

CERTIFICATE

It is certified that the work contained in the thesis titled **"Local Structure Variation, Phase Stability and Electrocatalytic Activity in Rocksalt and Spinel based MultiComponent (CoCuMgNiZn)-Oxide and its Derivatives"** by Saptarshi Mukherjee has been carried out under my supervision and that this work has not been submitted elsewhere for a degree.

It is further certified that the student has fulfilled all the requirements of Comprehensive, Candidacy and SOTA for the award of Ph.D. degree.

PROF. JOYSURYA BASU

(Supervisor)

Professor

PROF. N. K. MUKHOPADHYAY

(Co-supervisor)

Professor

Department of Metallurgical Engineering

Indian Institute of Technology

(Banaras Hindu University)

Varanasi

DECLARATION BY THE CANDIDATE

I, **Saptarshi Mukherjee**, certify that the work embodied in this Ph.D. thesis is my own bonafide work carried out under the joint-supervision of **Dr. Joysurya Basu** and **Prof. N.K. Mukhopadhyay** for a period from **January 2018 (Registration: December 27, 2017)** to **December 27, 2024** at the **Department of Metallurgical Engineering, Indian Institute of Technology (BHU)**, Varanasi, India. The subject matter embodied in this Ph.D. thesis has not been submitted elsewhere for the award of any other degree/diploma. I declare that I have faithfully acknowledged and given credits to the researchers wherever their works have been cited in my work in this thesis. I further declare that I have not wilfully copied any other's work, paragraphs, text, data, results, etc., reported in journals, books, magazines, reports, dissertations, thesis, etc., or available at websites and have not included them in this thesis and have not cited as my own work.

Date: December 27, 2024

Saptarshi Mukherjee

Place: Varanasi **(SAPTARSHI MUKHERJEE)**

CERTIFICATE BY SUPERVISORS

This is to certify that the above statement made by the candidate is correct to the best of my knowledge.

Joysurya Basu

Prof. JOYSURYA BASU
(Supervisor)

N. K. Mukhopadhyay

Prof. N.K. MUKHOPADHYAY
(Co-supervisor)

HEAD OF THE DEPARTMENT

COPYRIGHT TRANSFER CERTIFICATE

Title of the Thesis: Local Structure Variation, Phase Stability and Electrocatalytic Activity in Rocksalt and Spinel based Multi-Component (CoCuMgNiZn)-Oxide and its Derivatives

Candidate's Name: Saptarshi Mukherjee

COPYRIGHT TRANSFER

The undersigned hereby assigns to the Indian Institute of Technology (Banaras Hindu University), Varanasi all rights under copyright that may exist in and for the above thesis submitted for the award of ***Doctor of Philosophy***.

Date: December 27, 2024

Saptarshi Mukherjee

Place: Varanasi **(SAPTARSHI MUKHERJEE)**

Note: However, the author may reproduce or authorize others to reproduce materials extracted verbatim from the thesis or derivative of the thesis for author's personal use provided that the source and the Institute's copyright notice are indicated.

ACKNOWLEDGEMENT

"The known is finite, the unknown infinite; intellectually we stand on an islet in the midst of an illimitable ocean of inexplicability. Our business in every generation is to reclaim a little more land..." **-T. H. Huxley**

I must begin by trying to express my lifelong indebtedness towards my thesis supervisor Prof. Joysurya Basu, who also happens to be my friend, philosopher and guide. My greatest accomplishment by far, during this long arduous journey of earning my Ph.D. degree, is to come into correspondence with him. His scientific idiosyncrasies, thought provoking acumen and the sheer zeal to leave significant footprints in the profession, is unparalleled. I am most lucky to have gotten the chance to learn innumerable things from him, which is non-perishable and does not have a scope of decaying with time. The amount of guidance as well as free-hand extended by him in order for me to produce all the work pertaining to this thesis, has sculpted the researcher within me. His bold and fearless approach has inculcated a confidence in me to explore unchartered territories in the fascinating field of materials science and electron microscopy. Furthermore, his empathy and most amicable nature has helped me to grow both professionally and personally. I most sincerely take the pledge of walking down the roads of righteousness, discipline and honesty, which has been constantly and tirelessly advocated by him.

Prof. N. K. Mukhopadhyay, being my thesis co-supervisor, has been a fixed source of motivation and guidance, starting from my post-graduate journey. He is the first person who has introduced me to the nuances of physical metallurgy, which has consequently steered my scientific interests and career path. His classroom lectures on the subjects of materials characterization and intermetallics has immensely helped me throughout this tenure. I must also convey my deepest gratitude for the kindness extended by him during the tough times of lockdown and COVID aftermath. His financial support greatly helped me to attend several national and international conferences. I shall forever be indebted to him.

I sincerely thank my RPEC members, Dr. Imteyaz Ahmad and Dr. A.K. Mondal for their continuous constructive criticisms in the spirit of science, throughout these years. They have also highly facilitated the processing of every single official document during my Ph.D. span, despite all odds.

I cannot miss this opportunity to express my heartfelt thanks to Prof. R.K. Mandal, for being the epitome of support so that I may carry out research activities unperturbed. He is an academician par excellence and I am blessed to have learnt many things during my long association with him as his TA in several courses. Moreover, I am grateful to all the faculty members, present and past HoDs of our department for upholding a conducive research atmosphere in the department.

I take this scope of deeply thanking retired and emeritus faculties of our department Prof. S. Lele, Prof. G.V.S. Sastry, Prof. A.K. Ghose, Prof. S.N. Ojha, Prof. V. Singh among others. It is because of their teachings and encouragement that I have attempted to stand on the shoulder of giants in the field!

It is my good fortune that I got the prestigious opportunity to closely interact with Prof. D. Banerjee (IISc, Bangalore), Dr. P. Ghosal (DMRL, Hyderabad), Dr. K. Muraleedharan (CSIR-CGCRI), Dr. S. Bysakh (CSIR-CGCRI) and Prof. R. Ranjan (IISc, Bangalore) in matters of science and career advice.

I must acknowledge the tremendous faith put in me by faculties of my Alma Mater, Prof. P.P. Chattopadhyay, Prof. A. Basu Mallick, Prof. S. Chatterjee, Prof. S. Sadhukhan, Prof. S. Ghosh, Dr. D. Das, Dr. S.K. Ghosh, Dr. S. Kundu and Dr. T. Mandal of IIEST, Shibpur. In this regard, I also thank my teachers from school (BGKV, Kolkata), who laid the foundation stone of instilling a rational thinker in me.

I would like to take this opportunity to convey my thanks to all the lab staffs Ashok ji, Anjani ji, Ramashware ji, Kamlesh ji, Kamlaprasad ji, Chhotelal ji and Rajendra ji of this department for putting their best-efforts during times of serious crisis. I especially thank Lalit ji for maintaining the most sophisticated characterization facility of our department. I thank our department office staffs Patel ji, Rana ji, Aamir ji, Arun ji and Aftab ji, for handling and processing of all the required paperwork. I also sincerely thank staffs of CIFC of our institute, especially Anirban ji for his tremendous support during tough times.

I would also like to take this moment to thank all my department seniors Dr. M. Singh, Dr. V. Shivam, Dr. V.K. Pandey, Dr. V. Pandey, Dr. Y. Shadangi, Dr. A. Singh, Dr. A.S. Pal, Dr. A.K.L. Das, Dr. H. Jain among others. I sincerely thank my department colleagues and batchmates Soham, Satyam, Purnendu, Dr. R. Tandon, Dr. D. Bhuiyan, Dr. M.D. Rao for making my stay really cherishable. I am also thankful to my department juniors Rajdeep, Sai, Swarnendu, Latha, Snehita, Ashrita, Ravleen, Shivank, Urwashi, Priyatosh, Rajat, Ritwick, Anurag, Deep, Chayon and many others for a fond and memorable experience.

I will forever be grateful to almighty for bestowing me with the fortune of having several friends in my life, who are also my lifelines. They have immensely enriched my life.

Last but most importantly, I would like express my deepest gratitude towards all my family members for being constant motivators. I lost my grandparents when I was quite young, although I carry them in my heart and mind every single day. They have inculcated strong moral principles and values in me long back, which is continuously being germinated as I tread forward in life. Mr. Bimalendu Lahiri, being the brother of my maternal grandmother, has been a constant source of motivation and inspiration. My parents Dr. Pinaki and Mrs. Purabi Mukherjee are God-like figures in my life, for they have sacrificed on several fronts to make a good human being out of me. I just cannot thank them enough. I am also greatly indebted to them for finding my better-half while I was busy earning my Ph.D. degree. I must thank my gorgeous wife Megha for the unwavering support provided by her during a very tough phase. Her cheerful company always kept me focussed and determined. I thank my sister-in-law Alakta, my dearest nephew and best friend Bihan, my cousins Shovan, Sayan and my entire joint family for their relentless warmth and affection. Furthermore, I seek blessings from my late elder brother Debarshi, who in my most regretful opinion made the ultimate sacrifice so that I may shine perhaps. I terribly miss you and forever will……

To conclude, I take immense pride in remarking that my very existence thus far, has been shaped by the sum total of each and every contribution made by all the individuals mentioned above, the list of which is far from exhaustive.

TABLE OF CONTENTS

θ_B : Bragg angle

λ : Wavelength

G : Gibbs free energy

H : Enthalpy } *General Thermodynamics*

S : Entropy (total)

G_{mix} : Gibbs free energy of mixing

H_{mix} : Enthalpy of mixing } *Solution Thermodynamics*

S_{mix} : Entropy of mixing (configurational)

U : Internal Energy

P : Pressure

V : Volume

a : Lattice parameter

d : Inter-planar spacing

RS : Rocksalt

SP : Spinel

TEM : Transmission Electron Microscopy

SEM : Scanning Electron Microscopy

XRD : X-Ray Diffraction

SAED : Selected Area Diffraction Pattern

BF : Bright Field

CDF : Centered Dark Field

XEDS : X-ray Energy Dispersive Spectroscopy

LSV : Linear Sweep Voltammetry

CV : Cyclic Voltammetry

EIS : Electrochemical Impendence Spectroscopy

HEO : High Entropy Oxide

MCO : Multi Component Oxide

ESO : Entropy Stabilized Oxide

Figure 2.1: (a) Time-temperature diagram showing sintering of consolidated green pellets under various heat treatment schedules, which has been implemented for various multi-cationic compositions throughout the thesis. (b) Schematic showing mixing of powders in definite proportion, their consolidation followed by meticulous sample preparation for extensive characterization

Figure 2.2: Schematic of the electromagnetic (EM) spectrum

Figure 2.3: Schematic of the Real-space formulation of Braggs law for X-ray diffraction

Figure 2.4: Schematic representing various kinds of signal generation on interaction between x-ray and matter

Figure 2.5: Schematic of the TEM under (a) diffraction and (b) imaging mode

Figure 2.6: Schematic representing the diffraction setup in reciprocal space for (a) proper and (b) improper geometry

Figure 2.7: Schematic of the various kinds of signals that are produced from typical interactions between electron and matter

Figure 2.8: Schematic diagram of the four primary electromagnetic lens aberrations

Figure 2.9: Schematic representation of (a) Electrochemical Fuel cell (b) Li-ion battery and (c) Electrocatalysis for water-splitting

Figure 3.1: Experimentally observed x-ray powder diffraction pattern of (a-3C) ternary (CoMgNi)-oxide (a-4C) quaternary (CaCoMgNi)-oxide (a-5C) quinary (CaCoFeMgNi)-oxide after sintering at 1523 K for 10 h followed by water quenching. Simulated X-ray powder diffraction pattern of (b) cubic rocksalt structure with ~4.21 Å and ~4.78 Å lattice parameters (c) cubic spinel structure with ~8.35 Å and ~8.47 Å lattice parameters and (d) hexagonal phase with a ~2.94 Å, c ~5.28 Å lattice parameter and cubic Fe_2O_3 with ~9.39 Å lattice parameter. Experimental x-ray diffraction peaks are indexed with the same colour as that of the simulated patterns. Simulated patterns of cubic rocksalt, cubic spinel and hexagonal phase shows a strong match with the experimental patterns. Presence of cubic Fe_2O_3 cannot be ascertained in any of the experimental x-ray diffraction patterns

Figure 3.2: Experimentally observed powder x-ray diffraction patterns of as-mixed precursor oxide powders in equimolar ratio (in orange), the same as-mixed powder after dry ball milling for 40 h (in pink) and the pellet after sintering the green compacted ball milled powder at 1523 K for 10 h followed by water quenching (in red). In the sintered pellet cubic rocksalt phase, cubic spinel phase and the hexagonal phase can be indexed

Figure 3.3: Experimentally observed x-ray diffraction patterns of quinary equimolar (CaCoFeMgNi)-oxide pellet after sintering at 1523 K for 10 h (in red), 25 h (in green) and 100 h (in blue). In all the sintered pellets cubic rocksalt phase, cubic spinel phase and the hexagonal phase can be indexed

Figure 3.4: SEM-XEDS area map with Ca-K, Co-K, Fe-K, Mg-K and Ni-K in quinary equimolar (CaCoFeMgNi)-oxide after (A) sintering at 1523 K for 10 h and (B) sintering at 1523 K for 100 h followed by water quenching. (a) is the zoomed-in version of the area marked in (A) and (b) in the zoomed-in version of the area marked in (B). The XEDS maps are generated from the areas shown in (a) and in (b). In both the samples, two chemically segregated regions, one rich in Co, Mg, Ni ions and other rich in Ca and Fe ions can be observed

Figure 3.5: (a) Back scattered electron (BSE) image and X-ray energy dispersive spectrum (XEDS) from the points marked by s1-s6. Compositional contrast is observed in the BSE image. All the point XEDS from s1-s6 show the presence of all the elements, however in varying quantities. Compositions as obtained from XEDS are tabulated in the table below. It is again reconfirmed that Ca and Fe ion rich regions are relatively lean in Co, Mg and Ni ions and vice-versa. However, all the elements are present in all the phases. Based on the composition the predominant phase in different regions have been identified and their volume fraction as computed from the X-ray diffraction peak analysis is given in the table at the bottom of the figure

Figure 3.6: TEM (a, c) BF images and corresponding (b, d) single crystal diffraction patterns from z = [001] and z = [103] respectively in quinary equimolar (CaCoFeMgNi)-oxide after sintering at 1523 K for 10 h followed by water quenching. Thickness fringes in (a) and mottled contrast in (b) can be observed. The diffraction patterns in (b) and (d) are sharply defined. TEM (e, g) BF images and corresponding (f, h) single crystal diffraction patterns from z = [001] and z = [103] respectively in quinary equimolar (CaCoFeMgNi)-oxide after sintering at 1523 K for 100 h followed by water quenching. In the BF images in (e) and (g) fringe contrast within the mottled regions (marked with arrows) can be observed. In the diffraction patterns in (f) and in (h) arcs with modulated intensities can be observed

Figure 3.7: Selected area diffraction patterns from the quinary equimolar (CaCoFeMgNi)-oxide after sintering at 1523 K for (a) 10 h (b) 100 h followed by water quenching. In (a) experimentally observed d-spacings and their angular relationships are depicted. In (b) zone axis geometries are depicted. In (a) and (b) the data related to the cubic rocksalt phase, cubic spinel phase and the hexagonal phase are marked in green, yellow and white respectively. The cubic rocksalt phase, cubic spinel phase and hexagonal phase are oriented along z = $[\bar{1}11]$, z = $[\bar{1}11]$ and z = $[2\bar{1}\bar{1}0]$ respectively. Their orientation relationships are $[\bar{1}11]_{RS} \parallel [\bar{1}11]_{S}$ and $(220)_{RS} \parallel (2\bar{2}4)_{S}$; $[2\bar{1}\bar{1}0]_{H} \parallel [\bar{1}11]_{RS}$ and $(0002)_{H} \parallel (\bar{2}0\bar{2})_{RS}$; and $[2\bar{1}\bar{1}0]_{H} \parallel [\bar{1}11]_{S}$ and $(0002)_{H} \parallel (\bar{4}\bar{2}\bar{2})_{S}$ (RS: Rocksalt, S: Spinel; H: Hexagonal phase)

Figure 3.8: TEM (a) BF image and (b) corresponding rotationally aligned selected area diffraction pattern and (c) DF image using the superlattice reflection at ½[0002] (given at the inset in (c)) from the quinary equimolar (CaCoFeMgNi)-oxide after sintering at 1523 K for 10 h followed by water quenching. Linear fringes in (a) are from the twins and the

curvilinear contrast in (c) is from the APBs. The diffraction pattern in (b) indicates that the twins in (a) are compound deformation twins with s = $(2\bar{1}\bar{1}0)$, K_1 = (0002), η_1= $[0\bar{1}10]$, K_2 = $[10\bar{1}0]$ and η_2 = $[01\bar{1}1]$ as twin variants. (d) BF image (e) corresponding rotationally aligned diffraction pattern and (f) DF image from the quinary equimolar (CaCoFeMgNi)-oxide after sintering at 1523 K for 100 h followed by water quenching. The diffraction pattern in (e) is little off from the zone axis as shown in (b). All the spots perpendicular to the row of spots marked in cyan are split. The twins in (d) and in (f) are widely spaced

Figure 3.9: (a) Schematic representation of the mutually rotated domains in the intergrown helical arrangement with cubic rocksalt structure stacked along [001] direction. Possible composition modulation in each domain is marked with different colours. (b) $[2\bar{1}\bar{1}0]$ orthographic projection of the hexagonal phase with 2/3rd octahedral voids filled up. Cation ordering with vacancies along [0001] is depicted

Figure 3.10: (a) Schematic (202) || (422) interface between cubic rocksalt and cubic spinel phase. The interface is coherent. (b) schematic representation of (202) || (0002) interface between the cubic rocksalt phase with the hexagonal phase. The interface in semicoherent with quite minimal incoherency strain. The schematic diagrams are developed from the experimentally observed orientation relationships and the calculated crystallographic data from the diffraction patterns

Figure 4.1: (a) X-ray diffraction (XRD) patterns of (CoCuMgNiZn) ESO after sintering at 1323 K for 10 h followed by water quenching. The diffraction pattern in pink is from the sintered and quenched pellet and the pattern in blue is from its crushed powder. (b) Deconvolution of the XRD peaks from the crushed powder and (c) deconvolution of the XRD peaks from the pellet. Deconvoluted peaks can be matched with CoO, MgO and NiO.

Figure 4.2: (a) X-ray diffraction patterns (XRD) of (CoCuMgNiZn) ESO pellet after sintering at 1323 K for 10 h followed by water quenching (red), after sintering at 1323 K for 100 h followed by water quenching (pink) and after sintering at 1323 K for 10 h followed by furnace cooling (brown). (b) Superimposition of XRD peaks after three different thermal treatments. Long h of exposure at high temperature leads to a systematic left shift coupled with broadening and reduction in total integrated intensity

Figure 4.3: Scanning electron microscope (SEM) image and XEDS chemical maps of Co, Cu, Mg, Ni, Zn and the composite map of (CoCuMgNiZn) ESO pellet after (a) sintering at 1323 K for 10 h and (b) 1323 K for 100 h followed by water quenching. Fine scale segregation of Cu and Mg ions is evident in the maps. It is marked with arrows and delineated with dotted boundaries

Figure 4.4: Sintered and quenched equimolar quinary (CoCuMgNiZn)ESO exhibiting (a) Polycrystalline electron diffraction pattern with spotty rings which can be indexed to a FCC phase with a~4.23 Å lattice parameter whereas (b) and (c) are the corresponding BF-DF pair showing nano-crystallites of the rocksalt phase. It was recorded from the periphery of

the sample after ion-milling, making it necessary to revisit and optimize the electron thinning parameters to avoid such process-induced particle size refinement

Figure 4.5: (a-d) Electron diffraction patterns of (CoCuMgNiZn) ESO after sintering at 1323 K for 10 h followed by water quenching. The electron diffraction patterns are from (a) z=[012], (b) z=[$\bar{1}$14], (c) z=[$\bar{1}$23], (d) z=[$\bar{1}$12]. In the bright field image in (e) tweed contrast within the grain body and fringe contrast at the grain boundaries is observed. (f) Magnified image of the region marked with dotted square in (e). Tweed free region is marked with yellow lines

Figure 4.6: (a-d) Electron diffraction patterns, bright and dark field images of (CoCuMgNiZn) ESO after sintering at 1323 K for 10 h followed by water quenching. The diffraction pattern in (a) corresponds to z=[$\bar{1}$00] zone axis pattern of a cubic rocksalt structure. Diffused scattering, streaking and shape evolution (inset) of 02$\bar{2}$ type spot is observed. Extreme ends of the modulated spots are joined together to reveal the mutually rotated symmetry shapes. In the dark field image in (b) mutually intersecting non-orthogonal tweeds are observed. The electron diffraction pattern in (c) is from z=[011] zone axis of the same grain, where streaking and diffused intensity of the spots is observed. The bright field image in (d) shows the inter-penetrating tweeds

Figure 4.7: (a) Mutually rotated symmetry shapes as obtained from the electron diffraction pattern in Figure 5(a). The symmetry shapes may be separated into two groups with mutual relative rotation and with different c/a ratios. (b) Principal vectors from the symmetry shapes in (a) are plotted to reveal their relative rotation. (c) Mutually rotated symmetry shapes in (a) are superimposed to schematically generate the electron diffraction pattern in Figure 4.5(a)

Figure 4.8 (a-d): Electron diffraction patterns and TEM bright field images of (CoCuMgNiZn) ESO after sintering at 1323 K for 10 h followed by water quenching. Arcing in (a) z=[$\bar{1}$00] and (c) z=[$\bar{1}$12] electron diffraction patterns is associated with the mutual in-plane and out-of-plane rotation of domains. Intensity modulated arcs in each of the diffraction patterns are connected with dotted lines to reveal the symmetry shapes of the corresponding zone axes. Fringe contrast is observed in corresponding bright field images in (b) and (d). The fringes are marked with arrows

Figure 4.9: XRD patterns of (CoCuMgNiZn) ESO after sintering at 1323 K for 10 h followed by water quenching (in red) and after sintering at 1323 K for 10 h followed by ageing at 723 K for 120 h followed by water quenching (in blue). Anomalous intensity distribution and broadening of diffraction peaks after ageing is evident in the ESO

Figure 4.10: (a) z=[$\bar{1}$00] electron diffraction pattern, TEM (b-c) bright field images and (d) dark field image of (CoCuMgNiZn) ESO after sintering at 1323 K for 10 h, subsequent ageing at 723 K for 120 h followed by water quenching. In the diffraction pattern in (a),

asymmetrical diffused streaking of spots, splitting of spots is observed. In the bright field images (b-c) domain like structure with domain wall boundaries are observed. The domain wall boundaries are lightened up in the dark field image in (d) with g=020 diffraction spot

Figure 4.11: (a-b) Electron diffraction patterns from a different region of (CoCuMgNiZn) ESO after sintering at 1323 K for 10 h, subsequent ageing at 723 K for 120 h followed by water quenching. The diffraction pattern in (a) is inverted with respect to the diffraction pattern in (b). The patterns may be indexed with co-existent rocksalt phase and a spinel phase with a definite orientation relationship. The d-spacings, angular relationships and ratio of principal vectors are marked in (a). In (b) the diffraction spots corresponding to a rocksalt phase (green) and a spinel phase (yellow) are marked with different colours. The diffraction spots are connected with differently coloured dotted lines to bring out the zone axes symmetry shapes

Figure 4.12: (a) Schematic representation of structurally modulated domains in 2D and in 3D in the (CoCuMgNiZn) ESO. Structural modulation may be initiated with the chemical modulation in individual domains, which are represented with different colours. Structural modulation in 3D makes the ESO appear uniform in chemistry due to the overlap of domains with different chemistry. (b) Schematic representation of oriented growth of rocksalt phase and a spinel phase as obtained from the experimental diffraction patterns in Figure 10. The interface is coherent

Figure 5.1: (a) X-ray diffraction (XRD) patterns of equimolar (CoMgNi)-oxide powder in the as-mixed condition and after 5h, 15h, 40h of ball milling. (b) Simulated XRD pattern of cubic rocksalt (a ~ 4.2 Å) in red and cubic spinel (a ~ 8.1 Å) in blue respectively. (c) Magnified view of 311 peak of cubic spinel and 111 peak of cubic rocksalt in as-mixed condition and after 5h, 15h and 40h of ball milling (d) Magnified view of the evolution of 200 peak of cubic rocksalt phase in the as-mixed condition and after 5h, 15h and 40h of ball milling

Figure 5.2: X-ray diffraction (XRD) patterns of equimolar binary (MgNi)-oxide, (CoNi)-oxide and ternary (CoMgNi)-oxide powder after sintering at 1473 K for 10h followed by water quenching. In all three compositions cubic rocksalt phase forms as the major phase, however, with varying intensity ratios of 111 and 200 diffraction peaks

Figure 5.3: (a) X-ray diffraction (XRD) patterns of equimolar ternary (CoMgNi)-oxide powder (light green) and pellet (dark green) after sintering at 1473 K for 10h followed by water quenching. In the pellet, signature of cubic spinel phase is observed, which is absent in the powder. (b) Normalized intensity plots from the experimental XRD patterns of the powder (light green) and pellet (dark green). Compton modified scattering background is represented as bands with respective colours. Compton modified background for the powder being high, the low intensity spinel peak gets suppressed in the powder

Figure 5.4: (a-d) Bright field image and selected area diffraction patterns along z=[011], z=[125] and z=[013] zone axes from ternary equimolar (CoMgNi)-oxide after sintering at

1473 K for 10 h followed by water quenching. The diffraction patterns may be indexed to a cubic rocksalt phase (a ~ 4.2 Å) with diffuseness and occasional spot splitting. Mottled contrast associated with strain fields is observed in the bright field image. (e) Centred dark field image and complementary bright field image (inset) from the same ternary equimolar (CoMgNi)-oxide after sintering at 1473 K for 10 h followed by ageing at 723 K for 120 h, in which parallel fringe with alternating contrast is observed. (f) Magnified bright field image of (e) showing multiply oriented fringes with ~1.5-3.5 nm spacing between them

Figure 5.5: (a) Selected area electron diffraction pattern along z=[001] zone axis of (CoMgNi)-oxide after sintering at 1473 K for 10h followed by water quenching. Onset of splitting in the higher order spots (marked by dotted circles) is observed. (i-iv) Intensity distribution plots of 200 and 220 type spots are almost symmetrical. (b) Selected area electron diffraction pattern along z=[001] zone axis of (CoMgNi)-oxide after sintering at 1473 K for 10h, ageing at 723 K for 120h followed by water quenching. The diffraction spots are split and arced with modulation of intensity distribution. (v-viii) Intensity distribution plots of 200 and 220 type spots are not symmetrical with several maxima

Figure 5.6: X-ray diffraction (XRD) patterns of (CoMgNi)-oxide with systematic addition of Fe- and Mn-ions after sintering at 1473 K for 10h followed by water quenching. With systematic addition of Fe- and Mn-ions the major phase in the equimolar multicomponent oxide changes from cubic rocksalt phase to cubic spinel phase

Figure 5.7: (a, c) Selected area electron diffraction patterns along z=[001] and z=[$\bar{1}$14] zone axes respectively and (b, d) bright field images of the multicomponent equimolar (CoFeMgMnNi)-oxide after sintering at 1473 K for 10h followed by water quenching. Electron diffraction patterns are indexed to a cubic spinel phase (a~8.38 Å). In the bright field images mottled contrast with occasional fringe contrast (Figure 7d (inset)) is observed

Figure 5.8: Selected area electron diffraction patterns and bright field images of (CoFeMgMnNi)-oxide after sintering at 1473 K for 100h followed by water quenching.

The diffraction pattern in (a) is indexed to a cubic spinel phase, z=[$\bar{1}$14] zone axis along with a coexistent rocksalt phase, z=[001] zone axis. Indices of the diffraction spots, their angular relationships and ratios of principal vectors are given in (b), which is inverted with respect to (a). In the corresponding bright field image in (c), extensive fringe contrast (marked by arrows) within the mottled contrast is observed. The diffraction pattern in (e) is indexed to the same cubic spinel phase, z=[012] zone axis along with the coexistent cubic rocksalt phase, z=[013] zone axis. Indices of the diffraction spots, their angular relationships and the ratios of the principal vectors are given in (f), which is inverted with respect to (e). The corresponding bright field image in (d) shows domain like structure along with fringe contrast. Orientation relationship between the cubic spinel phase and the cubic rocksalt phase is evident

Figure 5.9: X-ray diffraction (XRD) patterns of (CoFeMgMnNi)-oxide and (CoCrFeMnNi)-oxide after sintering at 1473 K for 10h followed by water quenching. In

both of the multicomponent oxides cubic spinel phase is observed to be the predominant phase with systematic peak splitting and shouldering

Figure 5.10: (a-f) Bright field, centred dark field and selected area electron diffraction patterns of (CoCrFeMnNi)-oxide after sintering at 1473 K for 10h followed by water quenching. The diffraction pattern in (c) is indexed to a cubic spinel phase, z=[001] zone axis. The diffraction spots are diffused with streaking along mutually perpendicular 220 type directions (marked with arrows). In the bright field image in (a) and corresponding centred dark field image in (b) modulation and formation of nanodomains are observed (marked with arrows). In two-beam bright field image in (e) and in (f) modulation along 220 direction is observed. Corresponding two beam diffraction pattern is given in the inset of (e). Cross penetration of modulation leading to the formation of domains is shown in the high magnification image in (d)

Figure 5.11 (a-b): Projected interface structure diagram between cubic spinel phase and cubic rocksalt phase. The interface structure diagram has been developed based on the experimentally observed orientation relationship between the cubic spinel phase and the cubic rocksalt phase. The interfaces are semi-coherent in nature

Figure 6.1: LSV plots recording the current density as a function of applied voltage, calibrated against reduced hydrogen electrode. The response from each oxide is colour coded. The inset compares the electrocatalytic response from (CoCuMgNiZn)-oxide and its derivative (CoMgNi)-oxide after sintering and ageing heat treatments

Figure 6.2: Experimental XRD patterns from sintered and quenched equimolar, ternary (CoMgNi)-oxide (green), quaternary (CoMgMnNi0-oxide (purple), quinary (CoFeMgMnNi)-oxide (blue), (CaCoFeMgNi)-oxide (orange) and (CoCuMgNiZn)-oxide (magenta). Respective phases have been marked with different coloured symbols

Figure 6.3: SEM-SE micrographs, selected area diffraction pattern and TEM bright field/dark field images from sintered and quenched (a1-a3) (CaCoFeMgNi)-oxide, (b1-b3) (CoFeMgMnNi)-oxide, (c1-c3) (CoCuMgNiZn) ESO and (d1-d3) (CoCrFeMnNi) HEO respectively. The microstructural features are marked with arrows and indexing of diffraction patterns have been done employing different colour schemes

Figue 6.4: SEM-XEDS chemical mapping from (a1) sintered and quenched (CoMgNi)-oxide, (a2) sintered, aged and quenched (CoMgNi)-oxide, (b1) sintered and quenched (CoCuMgNiZn) ESO and (b2) sintered, aged and quenched (CoCuMgNiZn) ESO respectively. The quantification of the cation weight % has been provided in coloured boxes adjacent to the respective maps

Figure 6.5: (a) LSV response from sintered and quenched equimolar (CoMgMnNi)-oxide, (b) CV plots from the same oxide under varying scan rates and (c) schematic representing possible mechanism behind enhanced electrocatalytic activity in the same dual-phase oxide

Figure 6.6: (a) Overpotential plots for all the respective multicomponent oxides at 5 mA/cm^2 and (b) Tafel slopes for the same oxides. The histogram is accompanied with computed overpotential values at 1 mA/cm^2 (in white) and at 10 mA/cm^2 (in black). The Tafel slopes are marked over each oxide

Figure 7.1: Sintered and quenched pellet of equimolar ternary (CoMgNi)-oxide placed on an alumina tray filled with a mixture of alumina and graphite powder (a) before ageing treatment and (b) after ageing treatment. The obvious change in colour of the powder bed may easily be discerned

Figure A.1: Single-crystal spot electron diffraction patterns from several zone axis of a FCC structure ($u^2+v^2+w^2<22$). The patterns have been simulated with the help of JEMS software. The respective zone axis directions are marked with "ZA" on top of each pattern. The ratio of the principal vectors along with the interplanar angles are marked in the respective patterns.